J. Fluid Mech. (1976), *vol.* 75, *part* 3, *pp.* 525–544
Printed in Great Britain

Solutions of the Navier-Stokes equations for vortex breakdown

By W. J. GRABOWSKI
Flow Research Inc., Los Angeles, California 90045
AND S. A. BERGER
Department of Mechanical Engineering, University of California, Berkeley

(Received 23 October 1974 and in revised form 4 August 1975)

A numerical investigation of vortex breakdown has been undertaken in an attempt to understand its properties, and the mechanisms responsible for it. Solutions of the full steady axisymmetric Navier–Stokes equations for breakdown in an unconfined viscous vortex have been obtained for core Reynolds numbers up to 200, for a two-parameter family of assumed upstream velocity distributions. Diffusion and convection of vorticity away from the vortex core, and the strong coupling between the circumferential and axial velocity fields in highly-swirling flows, are shown to lead to stagnation and reversal of the axial flow near the axis. The various theories of vortex breakdown are considered in light of the present numerical solutions.

1. Introduction

Several theoretical interpretations of vortex breakdown have been proposed, both viscous and inviscid, with varying degrees of explanatory capability. They include the critical-state and finite-transition concepts of Squire (1960), Benjamin (1962, 1965*a*, *b*, 1967), Bossel (1967) and Randall & Leibovich (1973), and the so-called boundary-layer separation analogy of Gartshore (1962, 1963), Hall (1966, 1967) and Mager (1972). None of these has gained general acceptance, however, owing to both a lack of experimental confirmation and questions about the appropriateness of assumptions made in the analyses on which they are based. In response to this latter problem, a numerical investigation has been undertaken. In this study we present numerical solutions of the full Navier–Stokes equations for an unconfined axisymmetric viscous vortex, which exhibit many of the features associated with vortex breakdown. Solving the full equations numerically requires no assumptions about the flow, except that it be axisymmetric and laminar, and no approximations other than those inherent in the finite-difference formulation. The imposition of axisymmetry is an unfortunate economic necessity; nevertheless, based on this study and the previous analyses of others, the authors believe that the fundamental mechanisms responsible for the breakdown of an axisymmetric vortex flow are axisymmetric in nature. Solutions of the axisymmetric equations should, therefore, yield meaningful insight into the phenomenon. We shall assume that the flow is laminar, since, even if the assumption is not satisfied throughout the flow, there is reason to believe that the dynamics of breakdown can still be elucidated.

There are at least two previous studies of axisymmetric swirling flows exhibiting breakdown-like behaviour based on numerical solutions of the full viscous equations. Kopecky & Torrance (1973) (see also Torrance & Kopecky 1971) obtained numerical solutions for swirling flow in a constant-radius tube for Reynolds numbers, based on the mean axial velocity and tube radius, up to 1000. Unfortunately, they used a very coarse computational grid, and a form of upwind differencing which is only first-order accurate, and which introduces both false convection and diffusion (Torrance 1968). The solutions exhibit the pronounced retardation and stagnation of the axial flow characteristic of vortex breakdown for sufficiently high values of swirl. The breakdown bubbles obtained from these solutions are, however, very different in appearance from those observed experimentally by Harvey (1962) in a constant-radius tube and by Sarpkaya (1971*a*, *b*) in a diverging tube (see figure 2(*a*), plate 1). Lavan, Nielsen & Fejer (1969) also obtained numerical solutions for viscous swirling flow in a constant-radius tube. Although solutions were obtained that exhibited axial flow reversal, they were able to consider only very low Reynolds number flows (no greater than 20).

In an inviscid calculation of swirling flow in a tube, Bossel (1967) used superposition to obtain solutions of the stream function equation, which exhibit axial flow reversals and corresponding bubbles similar in appearance to some of those observed by Sarpkaya (1971*a*). The occurrence of these breakdown-like structures depended, however, not only on the assumed rotation rate of the flow upstream but also, quite strongly, on the assumed stream function distribution downstream; solutions exhibiting more than one retardation of the axial flow, as are observed in some experiments, were not obtained. The *ad hoc* nature of those downstream conditions makes the results difficult to interpret and, as Hall (1972) suggested, Bossel's main contribution is a demonstration of the consistency between abrupt changes in flow structures and the critical state.

Kopecky & Torrance (1973) made only a modest attempt to consider the various explanations and experimental observations of breakdown in the light of their numerical solutions; and Lavan *et al.* (1969) made no attempt whatsoever. Based on his results, Bossel (1967) described breakdown simply as a "phenomenon peculiar to supercritical rotating flows which have swirl values very close to the critical swirl value". In this study, special attention is paid to an evaluation of theories of breakdown in light of the numerical solutions presented herein.

2. Mathematical model

If we assume axial symmetry, and that the flow is steady in a co-ordinate system fixed with respect to the vortex generator (e.g. a lifting wing), the momentum equations for an incompressible flow in terms of cylindrical co-ordinates (r, θ, z), with corresponding velocity components (u, v, w), reduce to

$$u\frac{\partial u}{\partial r}+w\frac{\partial u}{\partial z}-\frac{v^2}{r}=-\frac{\partial p}{\partial r}+\frac{1}{Re}\left[\frac{\partial^2 u}{\partial r^2}+\frac{1}{r}\frac{\partial u}{\partial r}+\frac{\partial^2 u}{\partial z^2}-\frac{u}{r^2}\right], \tag{2.1}$$

$$u\frac{\partial v}{\partial r}+w\frac{\partial v}{\partial z}+\frac{uv}{r}=\frac{1}{Re}\left[\frac{\partial^2 v}{\partial r^2}+\frac{1}{r}\frac{\partial v}{\partial r}+\frac{\partial^2 v}{\partial z^2}-\frac{v}{r^2}\right], \tag{2.2}$$

and

$$u\frac{\partial w}{\partial r}+w\frac{\partial w}{\partial z}=-\frac{\partial p}{\partial z}+\frac{1}{Re}\left[\frac{\partial^2 w}{\partial r^2}+\frac{1}{r}\frac{\partial w}{\partial r}+\frac{\partial^2 w}{\partial z^2}\right]. \tag{2.3}$$

Mass conservation may be expressed as

$$\frac{1}{r}\frac{\partial(ur)}{\partial r}+\frac{\partial w}{\partial z}=0, \tag{2.4}$$

Lengths have been non-dimensionalized by a characteristic core radius δ, velocities by the free-stream axial velocity W_∞, and pressure by ρW_∞^2 after subtraction of p_∞, the uniform static pressure far from the vortex. The core Reynolds number is defined as $Re \equiv W_\infty \delta/\nu$. Since this system of equations is elliptic, appropriate conditions must be specified on the entire boundary of the domain; to avoid the difficulties associated with infinite domains, conditions that approximate those expected in a real vortex flow will be applied at the boundary of a sufficiently large finite region. Therefore, if we choose the core radius at $z = 0$ as δ, conditions are specified on the boundary of $0 \leqslant r \leqslant R$, $0 \leqslant z \leqslant L$ where R and L are much larger than one.

At the upstream boundary $z = 0$, the velocities are specified function of r. In particular we choose

$$u(r) = 0 \qquad \text{for} \quad 0 \leqslant r \leqslant R, \tag{2.5}$$

$$v(r) = Vr(2-r^2) \quad \text{and} \quad w(r) = \alpha+(1-\alpha)\,r^2(6-8r+3r^2) \qquad \text{for} \quad 0 \leqslant r \leqslant 1, \tag{2.6}$$

$$v(r) = V/r \quad \text{and} \quad w(r) = 1 \quad \text{for} \quad 1 \leqslant r \leqslant R. \tag{2.7}$$

α and V are defined below. At the downstream boundary, $z = L$, $0 \leqslant r \leqslant R$,

$$\frac{\partial u}{\partial z}=0, \quad \frac{\partial v}{\partial z}=0 \quad \text{and} \quad \frac{\partial w}{\partial z}=0. \tag{2.8}$$

At the axis, $r = 0$, $0 \leqslant z \leqslant L$,

$$u = 0, \quad v = 0 \quad \text{and} \quad \frac{\partial w}{\partial r}=0. \tag{2.9}$$

At the radial boundary, $r = R$, $0 \leqslant z \leqslant L$,

$$\frac{\partial(ur)}{\partial r}=0, \quad v = V/R \quad \text{and} \quad w = 1. \tag{2.10}$$

The upstream conditions at $z = 0$ were chosen to approximate the experimentally-measured velocity in vortex cores such as those of trailing vortices, and were used by Mager (1972) in his integral analysis of breakdown. V is the specified circumferential velocity at the core edge; it is equal to the circulation around the core after non-dimensionalization by $2\pi\delta W_\infty$. The cubic form of $v(r)$ allows solid-body-like rotation near the core centre, and a smooth transition to irrotational flow at the core edge. The circumferential velocity is a maximum at $r = \sqrt{\frac{2}{3}}$, and is equal to $1{\cdot}088\,V$. The quartic distribution of axial velocity in the core joins smoothly at the core edge with the uniform axial flow outside, and is such that shear vanishes at the axis. The parameter α is the ratio of the axial velocity at the core centre to the velocity in the free stream; setting α greater or less than one yields jet-like or wake-like profiles, respectively. Uniform axial flow results when $\alpha = 1$.

The conditions at $z = L$ are based on the assumption that far enough downstream axial gradients become negligibly small. This requirement is far less restrictive than an *a priori* specification of the solution downstream; and, although some small error is introduced, its effect upstream is limited if L is sufficiently large, as a numerical investigation described in §3 demonstrates. Similar conditions for primitive $(\mathbf{v}, p)$ variable formulations at outflow boundaries have been used by several authors (e.g. Fortin, Peyret & Temam 1971).

The axis $(r = 0)$ conditions result from mass conservation, and from the requirement that shear stress at the axis vanish. Conditions at $r = R$ are based on the assumption that phenomena occurring near the axis, including breakdown, have a negligible effect on the circulation and the axial velocity at large distances from the axis. The condition $\partial(ur)/\partial r|_{r=R} = 0$ is obtained from continuity and allows fluid flux through the boundary.

Co-ordinate transformation

Vortex breakdown is essentially localized in the vortex core, so that good resolution and a finely-spaced grid are required in and near the core. Concomitantly, the boundary conditions at $z = L$ and $r = R$ imply that derivatives in the axial direction sufficiently far downstream, and in the radial direction outside the core, become increasingly small with increasing r and z. A co-ordinate transformation, which stretches the region near the axis radially and the region near the upstream boundary axially, while contracting the more distant regions, is therefore advantageous. The transformations adopted are

$$y = \frac{1}{a}\ln(1 + r/b), \quad x = \frac{1}{c}\ln(1 + z/d).$$

These have been used in a number of problems (e.g. Pao & Daugherty 1969), and have been applied in this study to map the region $0 \leqslant r \leqslant R$, $0 \leqslant z \leqslant L$ onto $0 \leqslant y \leqslant \frac{1}{2}$, $0 \leqslant x \leqslant 1$. The values of a, b, c and d are determined from the specified values of R and L, and the desired number and distribution of grid points in each co-ordinate direction.

In terms of the transformed independent variables x and y, the transformed equations of motion are

$$fu\frac{\partial u}{\partial y} + sw\frac{\partial u}{\partial x} - hv^2 = -f\frac{\partial p}{\partial y} + \frac{1}{Re}\left[f^2\frac{\partial^2 u}{\partial y^2} + (g + hf)\frac{\partial u}{\partial y} + s^2\frac{\partial^2 u}{\partial x^2} + t\frac{\partial u}{\partial x} - h^2 u\right], \tag{2.11}$$

$$fu\frac{\partial v}{\partial y} + sw\frac{\partial v}{\partial x} + huv = \frac{1}{Re}\left[f^2\frac{\partial^2 v}{\partial y^2} + (g + hf)\frac{\partial v}{\partial y} + s^2\frac{\partial^2 v}{\partial x^2} + t\frac{\partial v}{\partial x} - h^2 v\right], \tag{2.12}$$

$$fu\frac{\partial w}{\partial y} + sw\frac{\partial w}{\partial x} = -s\frac{\partial p}{\partial x} + \frac{1}{Re}\left[f^2\frac{\partial^2 w}{\partial y^2} + (g + hf)\frac{\partial w}{\partial y} + s^2\frac{\partial^2 w}{\partial x^2} + t\frac{\partial w}{\partial x}\right], \tag{2.13}$$

and
$$hf\frac{\partial(u/h)}{\partial y}+\frac{\partial w}{\partial x}=0, \tag{2.14}$$

where $f(y) = \exp(-ay)/ab, \quad g(y) = -\exp(-2ay)/ab^2,$

$$s(x) = \exp(-cx)/cd, \quad t(x) = -\exp(-2cx)/cd^2, \quad \text{and} \quad h(y) = 1/r(y).$$

The transformed boundary conditions are as follows. For $x = 0$, $0 \leqslant y \leqslant \frac{1}{2}$,

$$u, \quad v \quad \text{and} \quad w \quad \text{are specified functions of} \quad r(y), \tag{2.15}$$

as given previously. For $x = 1$, $0 \leqslant y \leqslant \frac{1}{2}$,

$$\frac{\partial u}{\partial x}=0, \quad \frac{\partial v}{\partial x}=0 \quad \text{and} \quad \frac{\partial w}{\partial x}=0. \tag{2.16}$$

For $0 \leqslant x \leqslant 1$, $y = 0$,

$$u = 0, \quad v = 0 \quad \text{and} \quad \partial w/\partial y = 0. \tag{2.17}$$

For $0 \leqslant x \leqslant 1$, $y = \frac{1}{2}$,

$$u+\frac{f}{h}\frac{\partial u}{\partial y}=0, \quad v = V/R \quad \text{and} \quad w = 1. \tag{2.18}$$

3. Numerical method

Chorin's 'artificial compressibility' technique (Chorin 1967) was used to solve (2.11)–(2.14). The method is simple, efficient, and has a significant advantage over other primitive variable techniques, in that the solution of a Poisson equation for pressure, and consequently boundary conditions for the pressure, are not required. The method can be described as follows.

An auxiliary system of equations based on the general equations of motion for a steady, incompressible flow is introduced. The equations are

$$\frac{\partial \mathbf{v}}{\partial \tau}+\mathbf{v}.\nabla\mathbf{v} = -\nabla p+\frac{1}{Re}\nabla^2\mathbf{v}, \quad \gamma\frac{\partial p}{\partial \tau}+\nabla.\mathbf{v}=0. \qquad (3.1), (3.2)$$

This new system features a time-like dependence on a new variable τ, and the replacement of the kinematic constraint, that the velocity field be divergence-free, by (3.2), which permits a simple explicit variation of the pressure field. These auxiliary equations may be solved numerically from arbitrary initial conditions to a steady (i.e. τ-independent) limit, using any of a large variety of finite-difference schemes developed for initial-value problems. Then, since steady solutions of (3.1) and (3.2) necessarily satisfy the steady equations, the resulting numerical solution satisfies the original differential equations to the spatial order of accuracy of the particular difference scheme used. The artificial compressibility γ plays a role similar to a relaxation parameter, and vanishes from the steady solution. The technique has been successfully applied with various difference schemes to a number of problems (Chorin 1967; Plows 1968; Fortin *et al.* 1971).

The artificial compressibility method was applied to the transformed equations and boundary conditions, (2.11)–(2.18). The transformed auxiliary equations are (2.11)–(2.14) with the additional terms $\partial u/\partial\tau$, $\partial v/\partial\tau$, $\partial w/\partial\tau$ and $\gamma\,\partial p/\partial\tau$, respectively, An alternating-direction-implicit (ADI) finite-difference scheme (Peaceman & Rachford 1955) was used to compute the solution. (For details, see Grabowski 1974.) Centred differences were used for all spatial derivatives, including convective term. Pressure was defined on a staggered grid system, in order both to increase the accuracy of the scheme, and to avoid the necessity of calculating its variation at the boundaries. The spatial truncation error of the scheme is $O[(\Delta x)^2+(\Delta y)^2]$ and, except for the effects of first-order approximations for the derivative boundary conditions, the errors in the solutions are of the same order.

Analyses of linearized models of the Navier–Stokes equations suggest that a numerical solution should satisfy the criterion that the cell Reynolds number, Reh, where h is either Δx or Δy, be $O(1)$ (see e.g. Roache 1972), although the less restrictive requirement that $Reh^2 \sim O(1)$ is also sometimes suggested. We have found, nevertheless, as have others (see e.g. Hirsch & Rudy 1974) that it is possible to obtain numerical solutions for which the cell Reynolds numbers are an order of magnitude larger. Such is the case for all of the solutions presented here. While the penalty usually associated with large cell Reynolds number solutions is degradation of accuracy, the computational mesh used here is such that a greater number of grid points are present in those regions in which a lack of resolution and degradation of accuracy might be anticipated, somewhat alleviating this difficulty.

The results of the effort to determine an optimum value of the artificial compressibility were inconclusive, and γ was set to unity. Appropriate locations for the radial and downstream boundaries, R and L, were determined from a sequence of solutions at $Re = 100$. These showed that R could be set at 10, and L at 20, since the use of larger values changed the solutions insignificantly. Furthermore, these solutions agreed excellently with a solution for an infinite domain; the latter is a solution described in Grabowski (1974). (It was obtained using an infinite-to-finite transformation.) The grid system consisted of 1891 points with 61 points in the x direction, 31 in the y direction, such that 12 points were located in the intervals $0 \leqslant r \leqslant 1$, $0 \leqslant z < 1$. A time step of length 0·11, somewhat larger than the smallest real plane mesh width, was used, and convergence was assumed when changes in velocities were less than 0·0005 over 100 time steps. Typically, 2000 to 4000 time steps were required, and each computation required from two to four minutes of computer time on the Lawrence Berkeley Laboratory CDC 7600 computer.

4. Solutions and discussion

A total of thirty-nine solutions with various combinations of α, V and Re have been obtained, and are presented in Grabowski (1974). The largest Reynolds number at which solutions could be obtained over a reasonably wide range of α and V was 200. For qualitative purposes, several calculations at higher Reynolds numbers were performed using upwind differences to approximate the convection terms in the momentum equations.

Solutions

Figures 1 (*a*)–(*d*) display stream surface contours in an axial plane, calculated from solutions for $Re = 200$, $\alpha = 1$, and $V = 0{\cdot}85$, $0{\cdot}8944$, $1{\cdot}0$ and $1{\cdot}095$. The Stokes stream function was determined at the computational mesh points by numerical integration of the velocity components, and contours were then determined by interpolation. Since these solutions represent steady flows, a fluid particle entering the solution domain at $z = 0$ proceeds downstream, spiralling along the stream surface on which it enters.

For V less than about 0·85, the stream surfaces appear essentially cylindrical. Examples of such stream surface contours, obtained from solutions with $Re = 200$, $\alpha = 1$, and $V = 0{\cdot}63$ and $0{\cdot}80$, are presented in Grabowski (1974). As V increases beyond about 0·80, the stream surfaces become increasingly perturbed. At $V = 0{\cdot}85$, a divergence of the surfaces near the axis is apparent in the downstıeam portion of the domain (figure 1 (*a*)), and at $V = 0{\cdot}8944$ the perturbation has moved upstream, and has the form of a small, well-pronounced bulge (figure 1 (*b*)). Similar bulges were obtained experimentally by Sarpkaya (1971 *a*), analytically by Bossel (1967), and numerically by Torrance & Kopecky (1971).

The bulge moves upstream, and becomes a vortex breakdown at $V = 1{\cdot}0$ (figure 1 (*c*)). (For the sake of a precise criterion, we shall identify the occurrence of breakdown with stagnation on the axis.) The breakdown consists of a closed bubble or eddy of recirculating fluid, similar in shape to some of those observed by Sarpkaya (1971 *a*, *b*). The stream surfaces within the bubble represent negative values of the stream function, and stagnation points are located on the axis at the upstream and downstream ends of the eddy. Further increase in V, to 1·095, results in the more vigorous breakdown shown in figure 1 (*d*). The bubble is further upstream and is larger than in the previous case, although the two stagnation points have moved closer together. The initial expansion and contraction of the outer stream surfaces over the bubble are followed by a second expansion. The near entrainment into the bubble of the stream surface closest to the axis should especially be noted. Sarpkaya (1971 *a*) reported that fluid did not enter through the front of the bubble, but instead passed over it and entered from the back. Then, having mixed turbulently inside, fluid exited into a second core-like region. While turbulent mixing has not been included in this study, the similarity between figure 1 (*d*) and his photographs is striking. (See e.g. figure 2 (*a*), plate 1.) A superposition of the stream surfaces shown in figure 1 (*d*) and stream surfaces traced from figure 2 (*a*) is displayed in figure 2 (*b*) (plate 1). The figure suggests that the second stream surface expansion might be the axisymmetric counterpart to the spiral breakdown, which is almost always experimentally observed behind axisymmetric breakdown bubbles.

Figure 3 shows the variation of the velocity at the vortex axis obtained from the solutions for which stream surface contours were presented in figure 1, with the addition of the solutions obtained with $V = 0{\cdot}63$ and $0{\cdot}80$. Figures 4 and 5 display, respectively, the pressure calculated on the row of grid points nearest

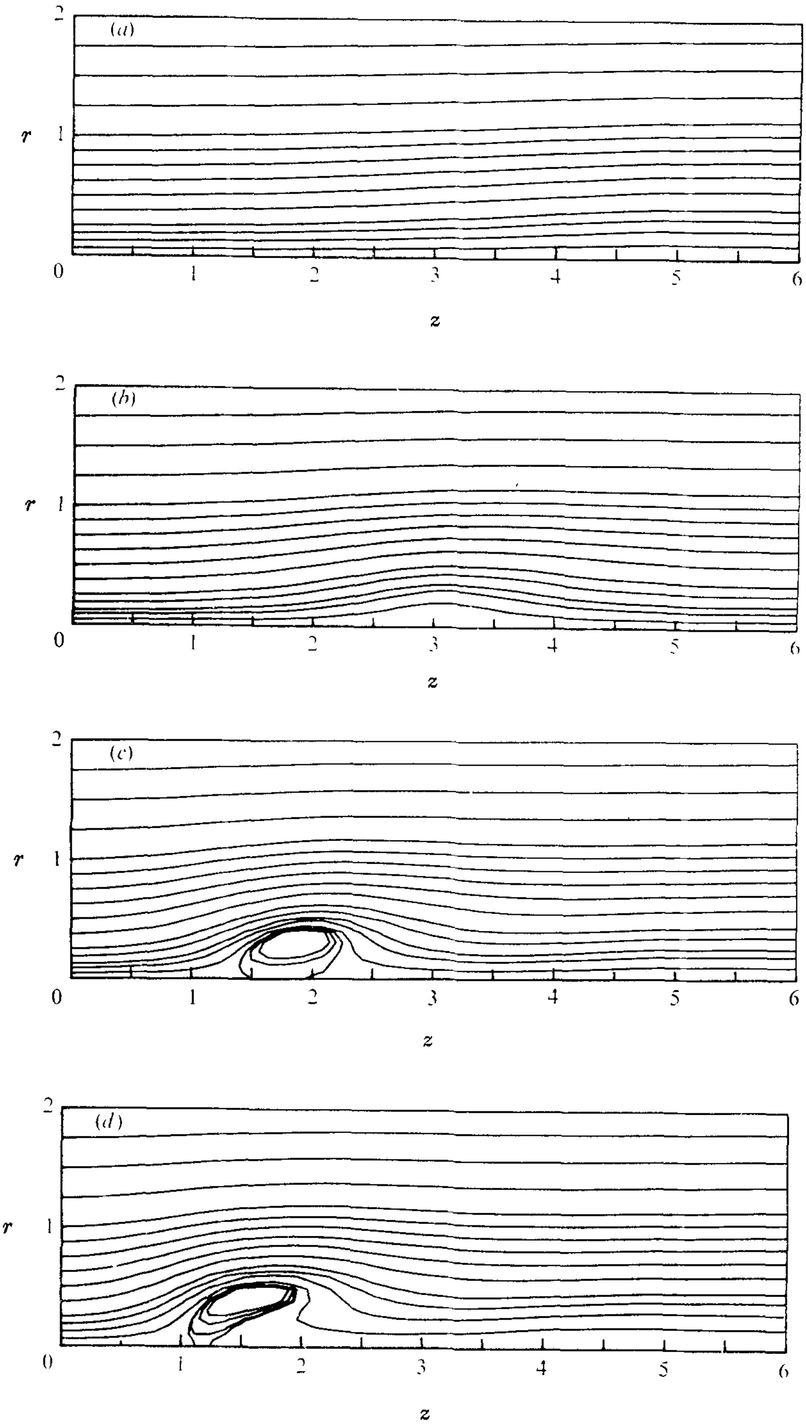

FIGURE 1. Stream function contours. $Re = 200$, $\alpha = 1$.

	(a)	(b)	(c)	(d)
V	0·85	0·8944	1·0	1·095

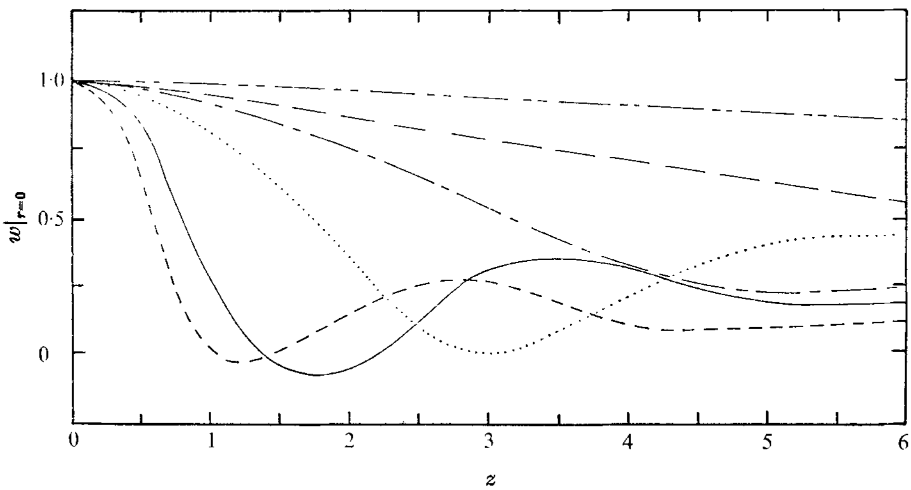

FIGURE 3. Velocity on vortex axis against axial location. $Re = 200$, $\alpha = 1$.

V	0·63	0·80	0·85	0·8944	1·0	1·095
	—··—	— —	—·—	······	——	----

the axis on which the pressure is defined,† and the swirl velocity at $r = \frac{1}{2}$ for the six solutions. Since the pressure in the vortex core will always be less than p_∞, the non-dimensional pressure is always negative. The axial variation of swirl at $r = \frac{1}{2}$ is characteristic of its variation within the core. Clearly, the effect of increasing swirl is to make the retardation of the axial flow, associated with the divergence of the stream surfaces, increasingly more pronounced. The large decreases in the minimum axial velocity, shown in figure 3, corresponding to small increases in V, demonstrate the highly nonlinear interaction between the swirl and axial velocities.

For low swirl ($V = 0{\cdot}63$, $0{\cdot}80$), the axial flow first gradually decelerates and, although not shown in figure 3, subsequently accelerates slowly to the free-stream velocity. The pressure deficit in the core increases asymptotically toward zero, and the swirl velocity slowly decreases.

In these low-swirl flows, axial gradients are much less than radial, so that the interaction of the pressure and the swirl may be examined using the quasi-cylindrical approximation $\partial p/\partial r = v^2/r$ (Hall 1966), which expresses the balance of the centrifugal acceleration of a fluid volume with the restraining pressure force. Integration with respect to r from the axis to radial infinity, where $p_\infty = \text{const.}$, followed by differentiation with respect to z, yields

$$\left(\frac{\partial p}{\partial z}\right)_{r=0} = -2\int_0^\infty \frac{v}{r}\frac{\partial v}{\partial z}\,dr.$$

Since viscous dissipation of swirl or, equivalently, diffusion of vorticity makes $\partial v/\partial z \leqslant 0$, the axial pressure gradient will be positive and will tend to decelerate the axial flow. However, $|v\,\partial v/\partial z|$ decreases continuously with z, so that shear

† We note that the pressure on the axis is not obtained, because in the finite-difference scheme pressures are calculated at computational cell centres.

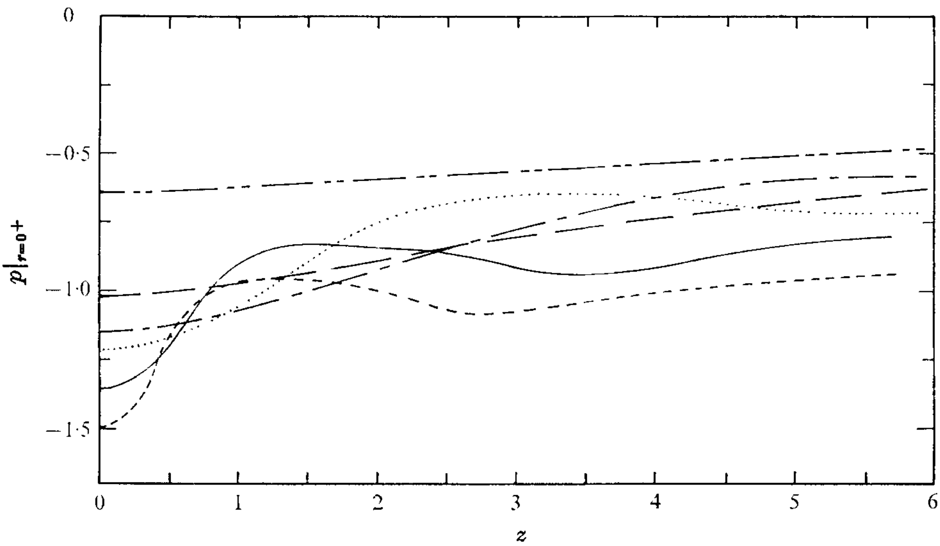

FIGURE 4. Pressure at $r = 0^+$ (about 0·04) against axial location. $Re = 200$, $\alpha = 1$. Symbol key as for figure 3.

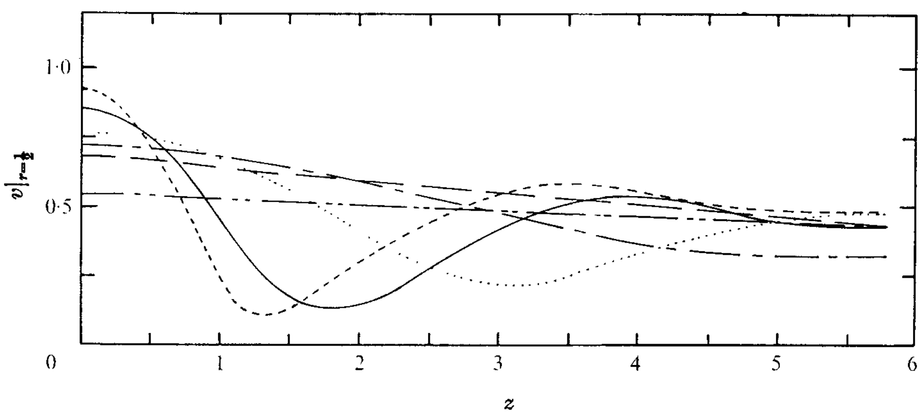

FIGURE 5. Swirl velocity at $r = 0{\cdot}5$ against axial location. $Re = 200$, $\alpha = 1$. Symbol key as for figure 3.

forces are eventually able, after the initial axial flow retardation, to accelerate the flow in the core to the free-stream velocity. For such a flow, the swirl velocity is essentially decoupled from the rest of the flow field, which it influences only through a small adverse pressure gradient.

The behaviour of the higher swirl solutions (i.e. $V = 0{\cdot}8944$, $1{\cdot}0$, $1{\cdot}095$), however, is quite different. In these cases, the distribution of swirl velocity cannot be decoupled from the rest of the flow field. Figures 6(*a*) and (*b*) display the axial and swirl velocity profiles, respectively, for the strongly swirling flow represented by the solution with $Re = 200$, $\alpha = 1$ and $V = 1{\cdot}095$. The axial velocity retardation arising from viscous dissipation of the swirl is large enough in these cases to require a significant amount of radial outflow. Since, except for

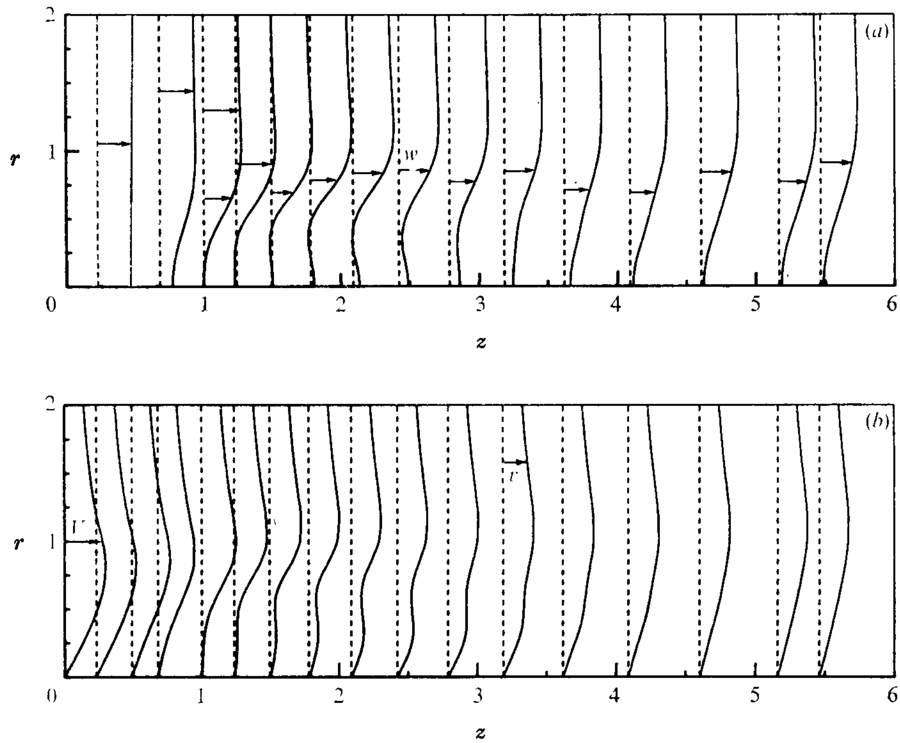

FIGURE 6. Velocity profiles for $Re = 200$, $\alpha = 1$, $V = 1{\cdot}095$. (a) Axial velocity. (b) Swirl velocity.

viscous effects, the angular momentum of a fluid particle is conserved as it moves radially outward, its swirl velocity must decrease. The bulge or breakdown bubble is thus a region of very low circumferential velocity. The reduction in swirl velocity resulting from radial outflow and diffusion is associated with a large increase in the pressure near the axis. But, since the adverse pressure gradient is negligibly small within the bubble, shear forces are able to accelerate the axial flow within the core; continuity then requires an inward motion of fluid toward the axis. In addition, owing to inertial effects, the fluid particles that were forced outward over the bubble move beyond the point of equilibrium between the local pressure gradient and the required centripetal acceleration; this also leads to an inward motion toward the axis. The combined inward flow, due to both of these factors, leads to an increase in swirl velocity, in order to satisfy angular momentum conservation, and to a corresponding decrease in pressure, which enhances the axial flow acceleration. Diffusion of vorticity once again becomes significant, reducing the swirl velocities near the axis, and, as before, inertia causes the now inwardly moving particles to overshoot the radial equilibrium position and, therefore, to begin moving outward. Both of these lead to an adverse pressure gradient which, for the case $\alpha = 1$, $V = 1{\cdot}095$, nearly stagnates the axial flow once more. Obviously, while the dynamics are such that this process can repeat itself, diffusion and dissipation seem to bring it to an end quickly.

Figures 7(*a*)–(*e*) display the stream function contours for several other solutions. Comparison of figures 7(*a*), (*b*) and 1(*b*) shows the effect of α and, hence, axial momentum on the location and size of breakdown. As α is increased from 0·3 (figure 7(*a*)) to 0·6 (figure 7(*b*)), the bubble becomes smaller and is located further downstream. For $\alpha = 1{\cdot}0$ (figure 1(*b*)) it is reduced to a bulge, while for $\alpha = 1{\cdot}4$ (not shown here) the stream surface contours appear as essentially straight lines. Figure 7(*c*), which shows the stream function contours obtained from the solution with $Re = 200$, $\alpha = 0{\cdot}6$ and $V = 1{\cdot}095$, should be compared with figure 1(*d*). At the lower value of α, the bubble is further upstream and the second retardation consists of a small region of reversed flow. Finally, figures 7(*d*) and (*e*) display the contours obtained with $Re = 100$, $\alpha = 1$ and $V = 1{\cdot}095$ and 1·342. The breakdown bubble is very large in the latter figure, and is followed by a low-velocity region in which a second reversal occurs. This rather large low-velocity region may represent an early stage in the development of a very large scale flow reversal, similar to that obtained by Harvey (1962).

Discussion

Many of the theories of vortex breakdown lead to criteria for its onset that are based on the swirl angle, defined as $\tan^{-1}(v/w)$, upstream of breakdown. Swirl angles immediately upstream of breakdown were observed by Harvey (1962) and Sarpkaya (1971*a*, *b*) to be between about 40 and 50°. Theoretical predictions of the maximum swirl angle have been based on critical-state concepts (Squire 1960). In these breakdown is related to the existence of a critical state, in which a standing cylindrical wave can first be maintained. Theoretical predictions have also been based on the finite-transition concept (Benjamin 1962, 1965*a*, *b*, 1967). This views breakdown as a transition between two conjugate flow states, in analogy with the hydraulic jump phenomenon.† These predictions vary from 45 (Squire 1960) to 62·5° (Bossel 1967), depending on the velocity profiles assumed for analysis. This is a considerable range of variation since the maximum value of v/w varies, therefore, from 1·0 to 1·92. Based on the numerical solutions, the swirl angles at $z = 0$ corresponding to solutions exhibiting stagnation on the axis vary between about 44 and 51°, as shown in figure 8.‡

Mager (1972) used Benjamin's (1962) test equation to evaluate the criticality of flows described by the velocity profiles assumed at $z = 0$ in the present study. Flow states thus identified with Benjamin's super- and subcritical regimes, and the critical state that separates them, are shown in an α, V plane in figure 9. Superposed on that figure are the values of α and V for which solutions were obtained with $Re = 200$. (In the interest of clarity, the α and V for solutions with $Re = 100$ are not shown.) The figure also indicates which solutions exhibit reversed axial flow (or in the case of the solution obtained with $\alpha = 1$ and

† Benjamin (1962) defines a supercritical flow as one that cannot support axisymmetric standing waves, and a subcritical flow as one that can support such waves. Squire's (1960) critical state is the borderline state. The conjugate flow pair of the finite-transition theory consists of a super- and a subcritical flow, and the transition occurs from the former to the latter.

‡ Swirl angles at $z = 0$ are used here for comparison with experimental swirl angles since in these solutions breakdown occurs very near the initial station.

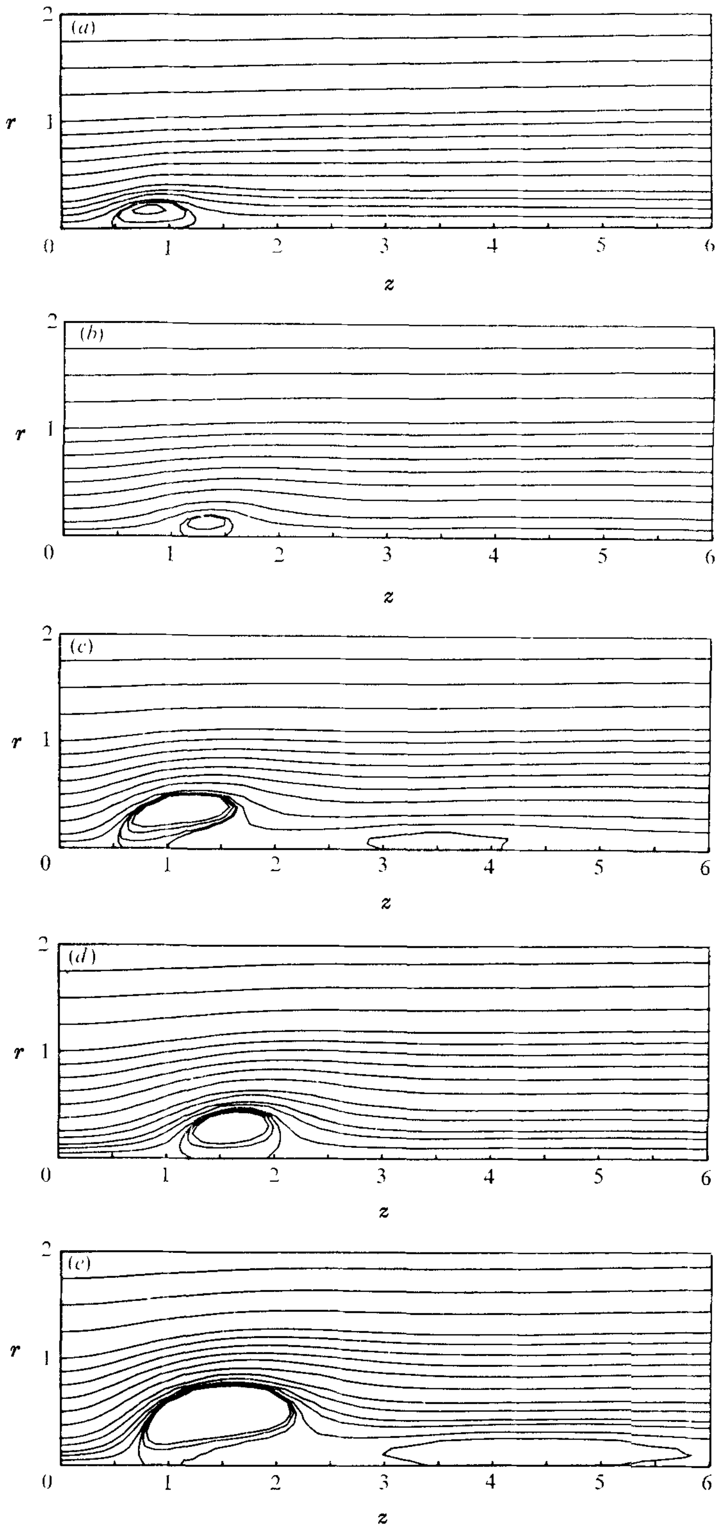

FIGURE 7. Stream function contours for several other solutions.

	(a)	(b)	(c)	(d)	(e)
Re	200	200	200	100	100
α	0·3	0·6	0·6	1·0	1·0
V	0·8944	0·8944	1·095	1·095	1·342

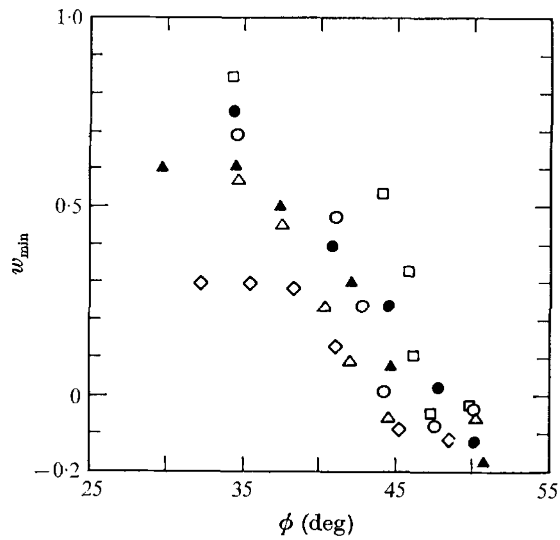

FIGURE 8. Minimum axial velocity on axis against upstream maximum swirl angle. Open symbols, Re = 200; closed, Re = 100.

α	0·3	0·6	1·0	1·4
	◇	△	○	□

$V = 0{\cdot}8944$, reduction to less than 1 % of the free-stream axial velocity). Based on these results, the breakdown solutions with $Re = 200$, $\alpha = 0{\cdot}3$, $V = 0{\cdot}8944$, with $Re = 200$, $\alpha = 0{\cdot}6$, $V = 1{\cdot}095$ and with $Re = 100$, $\alpha = 1$, $V = 1{\cdot}342$, presented earlier, were all obtained with subcritical upstream conditions. In general, no correlation was found between the occurrence of breakdown and the super- and subcriticality of the upstream conditions as represented in figure 9, whereas the finite-transition theory requires that the flow upstream of breakdown be supercritical. The finite-transition theory, as it is currently formulated (see e.g. Hall 1972), seems unable, therefore, fully to account for the phenomenon.† The subcritical upstream conditions for these solutions, however, are not very far in the α, V plane from the boundary separating the sub- and supercritical regimes; and, since Benjamin's test criterion strictly applies only to parallel and inviscid flows, neither of which is the case here, the possibility must be admitted that upstream conditions which according to Mager are subcritical could, in fact, be slightly supercritical in terms of being incapable of supporting axisymmetric standing waves.

Computations with values of V large enough to ensure highly subcritical upstream conditions failed to converge. The authors believe that this is not related to the nature of subcritical flows, since calculations with large values of α (greater than 1·4), and V large enough to be of interest in this study, also did not

† In most of the cases exhibiting breakdown, the breakdown occurs very close to the initial station. It is therefore possible that, for the initially-subcritical flows, our numerical results represent the completion of a breakdown which has occurred upstream of our initial station, and that that breakdown developed from supercritical upstream conditions. (This interesting possibility was raised by a referee.)

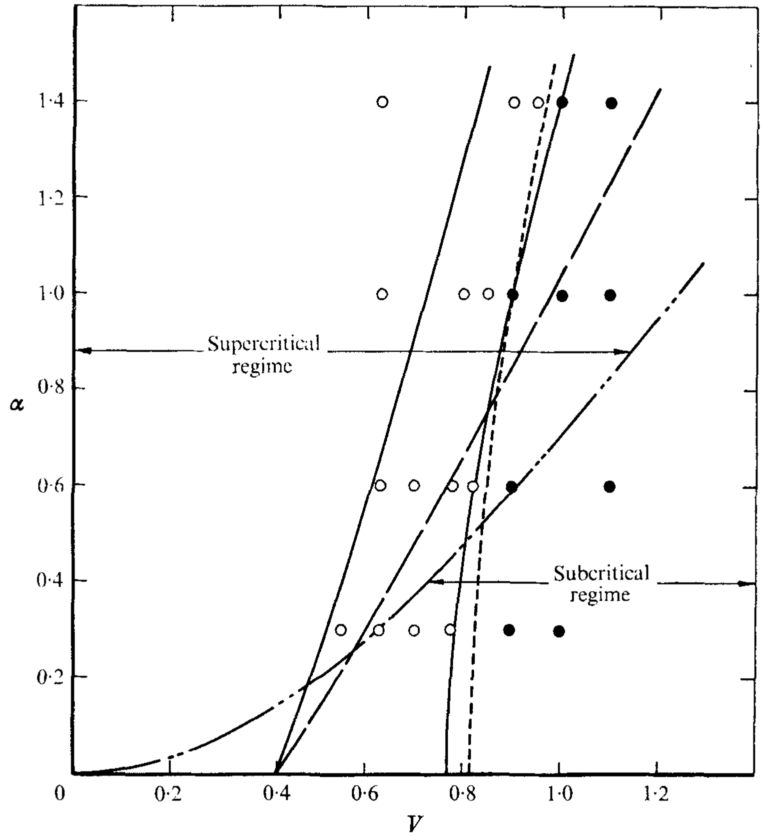

FIGURE 9. The α, V plane. Closed and open symbols represent upstream conditions for which flow reversal respectively was and was not obtained. —·—·—, critical-state locus; — —, Mager's discontinuity locus; ---, interpolated curve representing upstream conditions expected to yield solutions with a minimum axial velocity of zero.

converge. The upstream conditions in these cases were highly supercritical (again on the basis of figure 9). The failure of the calculations with apparently highly super- and subcritical upstream conditions is probably related to the fact that, for large α and V, the effective Reynolds number of the flow (i.e. the characteristic ratio of convective to diffusive momentum transport) may be significantly larger than the nominal (core) Reynolds number, and require a finer mesh system. Numerical calculations at a fixed core Reynolds number could thus suffer degradation of accuracy, and could eventually fail as α or V are increased.

An idea originally suggested by Gartshore (1962, 1963), and further elucidated by Hall (1967), is that the location and occurrence of vortex breakdown can be predicted by the appearance of discontinuities in solutions of the quasi-cylindrical equations: a parabolic, boundary-layer-like system, valid for vortex flows, in which radial gradients are much larger than axial gradients. This was taken up by Mager (1972). A modification of Mager's approach in fact yielded predictions of the location of breakdown in diverging tubes under a wide range of conditions, which are in very good agreement with experimental results (Sarpkaya 1974). In

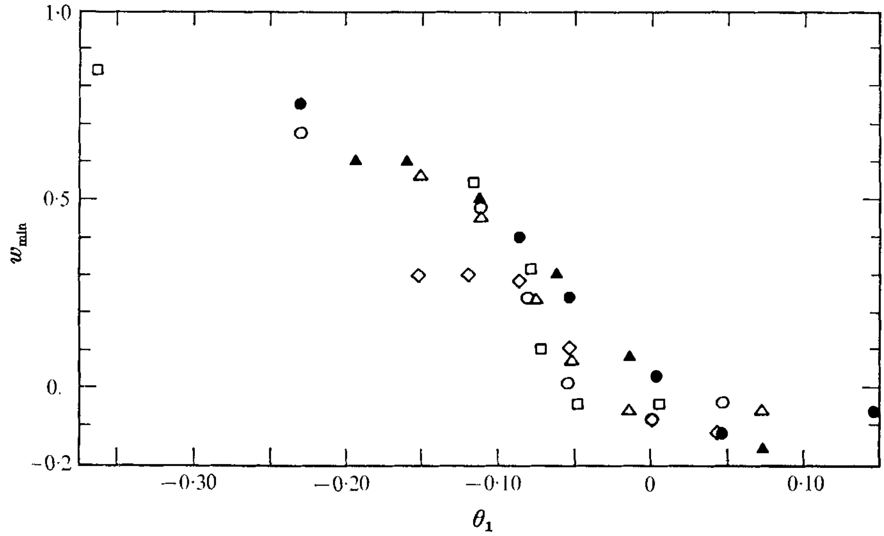

FIGURE 10. Minimum axial velocity on axis against parameter θ_1. Symbol key as for figure 8.

Mager's integral analysis, α and V are form factors for velocity profiles assumed to approximate the axial and circumferential velocity distributions throughout the core. The integral approach then consists of the determination of α and V as functions of z from their given upstream values. The analysis indicates that, if a certain parameter θ_1 is less than a critical value $\theta_1^* = -0{\cdot}163989$, then there will be a continuous solution; however, if $\theta_1 > \theta_1^*$, discontinuities will arise, marked by the appearance of infinite gradients, regardless of the apparent sub- or supercriticality of the upstream flow.† These discontinuities are assumed to represent the onset of breakdown. The parameter θ_1 is the axial momentum flux deficit in the core, which is an invariant in any quasi-cylindrical vortex flow, plus a term dependent on the fixed vortex circulation. θ_1 is determined from the conditions at $z = 0$, and in general decreases with the assumed value of α and increases with the assumed value of V. The locus of α and V for which $\theta_1 = \theta_1^*$ is shown in figure 9, along with a line representing the values of α and V at which the integral solutions were found to become discontinuous. The qualitative similarity between this discontinuity curve and that representing Benjamin's critical state is not unexpected, in the light of Hall's (1972) demonstration of the equivalence of the critical state and the condition that the inviscid cylindrical stream function admit discontinuous solutions.

The relationship between the calculated minimum axial velocity on the axis and θ_1 is indicated in figure 10 for all solutions with $Re = 100$ and 200. A correlation in these results, except for the two $\alpha = 0{\cdot}3$ cases, is apparent, and is in accord with Mager's integral analysis. The two $\alpha = 0{\cdot}3$ cases are anomalous in that the minimum axial velocity occurs at the initial station, $z = 0$. Interpolation for the value of θ_1 which corresponds, for any α, to a minimum velocity of zero

† The particular value of θ_1 at which discontinuities will first arise would be expected to vary with the assumed form of the velocity profiles.

yields for $Re = 200$ a limited range of θ_1, from $-0{\cdot}06$ for $\alpha = 1{\cdot}4$ to $-0{\cdot}025$ for $\alpha = 0{\cdot}3$. Thus, it seems that the occurrence of breakdown in the numerical solutions may be approximately correlated with a critical value of θ_1, which for $Re = 200$ is about $-0{\cdot}05$, as suggested by Mager's analysis. A line representing the locus of α and V for which $\theta_1 = -0{\cdot}05$ is included in figure 9. Also drawn in that figure is a very similar curve, determined by interpolation, representing the values of α and V for which numerical solutions with $Re = 200$ are expected to predict a minimum axial velocity of zero. Numerical solutions with upstream conditions (i.e. α and V) to the right of this 'incipient breakdown' locus are expected to exhibit breakdown.

The minimum axial velocities for the $Re = 100$ cases also collapse onto a single curve. The amount of scatter in these results is less than the $Re = 200$ cases, perhaps because the solutions at this lower Reynolds number may tend to be more accurate. The critical value of θ_1 is about $0{\cdot}01$ for both $\alpha = 0{\cdot}6$ and $1{\cdot}0$. Should the trend of decreasing critical θ_1 with increasing Re continue, the critical θ_1 could possibly approach Mager's prediction for very high Reynolds numbers. This, however, is only a hypothesis. Also, θ_1^* is the value of θ_1 at which a large axial gradient will appear, and it might be less than the value corresponding to axial flow reversal.†

Figures 11 (*a*) and (*b*) show a comparison, for several Reynolds numbers, of the axial variation of $w|_{r=0}$ for $\alpha = 1$, and $V = 0{\cdot}63$ and $0{\cdot}8944$, respectively. The calculations with $Re = 500$ and 1000 were performed using upwind differencing and are probably only suggestive of the actual flows. Figure 11 (*a*) shows that the very mild axial flow retardation in the solutions with $V = 0{\cdot}63$ becomes less pronounces as Re increases. This is in accord with the analyses of both Gartshore (1962, 1963) and Mager (1972), in which Re enters the solution only as a scale factor for z. Figure 11 (*b*), however, suggests that solutions which exhibit breakdown at relatively low Reynolds numbers should continue to do so as Re is increased. It is therefore expected that, while this study has obtained quantitative information for relatively low Reynolds numbers only, the conclusions reached here can be extended to higher Reynolds number flows.

Forms of breakdown

In order to explain the appearance of an axisymmetric bubble followed by a spiral breakdown in highly swirling flows, and the appearance of only the spiral in flows with less swirl, Mager (1972) argued that the axisymmetric bubble results from a cross-over, ahead of the discontinuity, of the solution from the upper to the lower branch of an integral curve with the same value of θ_1. It was suggested that this cross-over is analogous to Benjamin's finite transition; that the discontinuity appears physically as the spiral breakdown; and that the crossover, if it occurs, appears as the axisymmetric bubble. Such a hypothesis does not explain Sarpkaya's (1974) accurate predictions of the location of both axisymmetric and spiral breakdowns, based only on the appearance of discontinuities. The

† We note in this connexion that, at the axial locations at which the various quasi-cylindrical solutions (Hall 1967; Bossel 1971; Mager 1972) fail, the axial velocity is generally greater than zero by a significant fraction of the free-stream axial velocity.

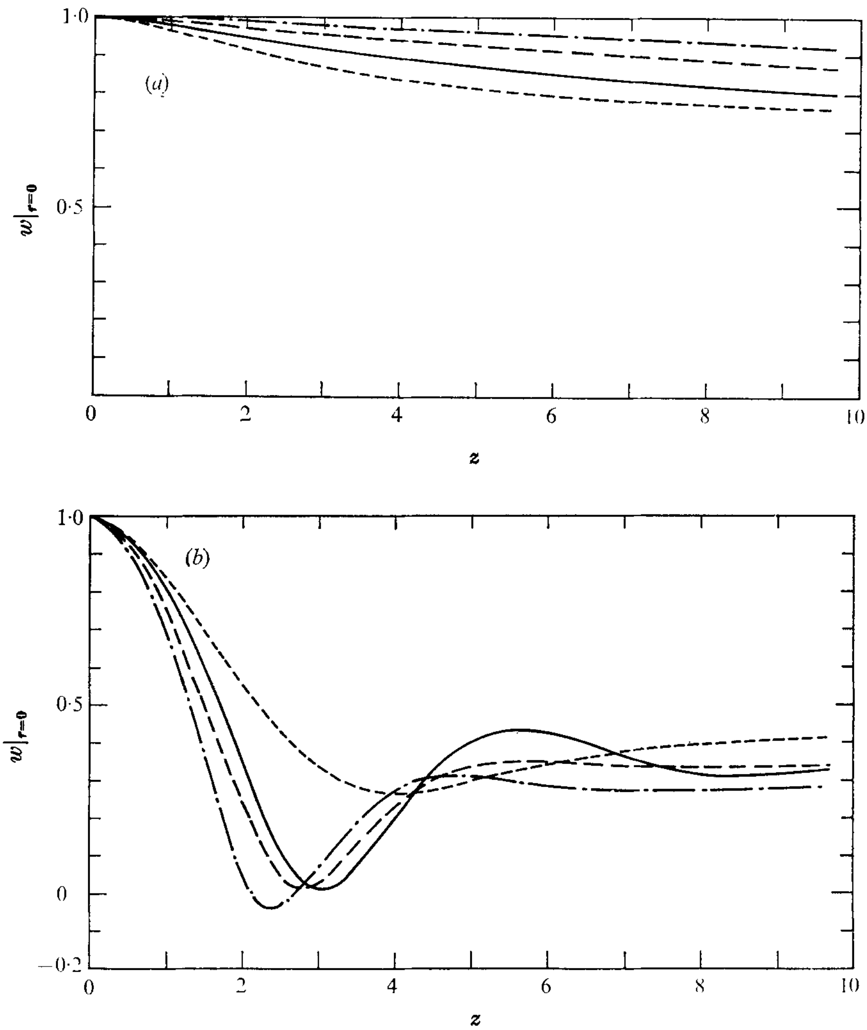

FIGURE 11. Velocity on vortex axis for $\alpha = 1$ and several Reynolds numbers. (a) $V = 0{\cdot}63$; (b) $V = 0{\cdot}8944$.

Re	100	200	500	1000
	------	————	— — —	— · —

following comments represent, we believe, an explanation of the various forms of vortex breakdown consistent with the numerical solutions obtained in this study and the observations of Sarpkaya (1971*a*, *b*).

In flows where the swirl velocities are not large, the axial retardation may be such as to produce a region of flow in the vortex core unstable to certain spiral disturbances. The introduction of such a disturbance could then result in the development of a spiral breakdown. Sarpkaya (1971*b*) has, in fact, suggested that the spiral is the result of an instability in flows with moderate swirl; and the agreement pointed out by Ludwieg (1965) between predictions based on his theory that breakdown is the result of a spiral instability and the measurements of Kirkpatrick (1964) and Hummel (1965) would then be explained. As Hall (1972) suggested, however, these instabilities might not occur in flows with high swirl, and the retardation of the axial flow would then result in the axisymmetric bubble. For large values of V, however, the second retardation that occurs in the numerical solutions may result in a region of flow behind the bubble unstable to a spiral disturbance, in which case the flow could appear as an axisymmetric bubble followed by a spiral. Such a possibility was originally suggested by Benjamin (1967).

5. Conclusions

Numerical solutions of the Navier–Stokes equations for axisymmetric swirling flows were obtained, and were shown to exhibit many of the characteristics of vortex breakdown. They suggest that the occurrence of breakdown can be correlated with the value of a parameter which is a measure of the axial momentum flux deficit, or flow force deficiency, in the vortex core. Solutions exhibiting breakdown were obtained with upstream conditions which, according to Benjamin's criterion, are subcritical. The finite-transition theory, as it is currently formulated, therefore, seems inconsistent with the numerical results, although a reformulation to include the effects of the large axial gradients encountered in them is required before a complete comparison can be made.† In this connexion, the reader should recall the comments concerning our inability to obtain solutions for upstream conditions that are highly super- or subcritical. Although we suggested that this difficulty is associated with purely numerical considerations, we cannot rule out the possibility that, in the case of subcritical upstream conditions, the inability to obtain solutions is, in fact, associated with the particular characteristics of subcritical flows.

In the absence of an externally-imposed pressure gradient or flow divergence, breakdown results from the diffusion and convection of vorticity away from the vortex core. When the axial momentum of the flow near the axis is sufficiently small compared with the resulting pressure forces, the retardation is sufficient to result in stagnation and flow reversal. The calculations demonstrate that the nonlinear coupling between the axial and swirl velocities leads to a very rapid onset of breakdown when it occurs, and they suggest, as Hall (1972) proposed, that breakdown is a critical state to which a vortex with sufficient swirl can be reduced by diffusion of vorticity, flow divergence and pressure forces.

Finally, it was suggested that retardations which appear in solutions with moderate values of swirl might be unstable to spiral disturbances. In that case, the physical manifestation of breakdown might be the single asymmetric spiral observed in experiments. Of particular significance is the fact that the numerical solutions for large values of swirl exhibit a second axial flow retardation. If the first retardation were stable and the second unstable, the physical manifestation might be the axisymmetric bubble followed by a spiral as observed in experiments.

† See also the footnote on p. 538.

The major part of this work was supported by NASA grant NGR 05-003-451 at the University of California, Berkeley, and was performed as part of the Ph.D. requirements of one of the authors (W. J. G.). The authors wish to express their thanks to the referees for their helpful comments and criticisms.

REFERENCES

Benjamin, T. B. 1962 *J. Fluid Mech.* **14**, 593.

Benjamin, T. B. 1965*a* *Trans. A.S.M.E., J. Basic Engng*, **87**, 518.

Benjamin, T. B. 1965*b* *Trans. A.S.M.E., J. Basic Engng*, **87**, 1091.

Benjamin, T. B. 1967 *J. Fluid Mech.* **28**, 65.

Bossel, H. H. 1967 *University of California, Berkeley, College of Engineering, Rep. AS*-67-14.

Bossel, H. H. 1971 *A.I.A.A. J.* **9**, 2027.

Chorin, A. J. 1967 *J. Comp. Phys.* **2**, 12.

Fortin, M., Peyret, R. & Temam, R. 1971 *J. Méc.* **10**, 357.

Gartshore, I. S. 1962 *N.R.C. (Canada) Aero. Rep.* LR-343.

Gartshore, I. S. 1963 *N.R.C. (Canada) Aero. Rep.* LR-378.

Grabowski, W. J. 1974 *University of California, Berkeley, College of Engineering, Rep. FM*-74-6.

Hall, M. G. 1966 *Prog. Aero. Sci.* **7**, 53.

Hall, M. G. 1967 *Proc. Heat Transfer Fluid Mech. Inst.* p. 319.

Hall, M. G. 1972 *Ann. Rev. Fluid Mech.* **4**, 195.

Harvey, J. K. 1962 *J. Fluid Mech.* **14**, 585.

Hirsch, R. S. & Rudy, D. H. 1974 *J. Comp. Phys.* **16**, 304.

Hummel, D. 1965 *Z. Flugwiss.* **13**, 158.

Kirkpatrick, C. L. I. 1964 *Brit. A.R.C. CP* 821.

Kopecky, R. M. & Torrance, K. E. 1973 *Computers and Fluids*, **1**, 289.

Lavan, Z., Nielsen, H. & Fejer, A. A. 1969 *Phys. Fluids*, **12**, 1747.

Ludwieg, H. 1965 *Z. Flugwiss.* **13**, 437.

Mager, A. 1972 *J. Fluid Mech.* **55**, 609.

Pao, Y. H. & Daugherty, R. J. 1969 *Boeing Scientific Res. Lab. D*1-82-0822.

Peaceman, D. W. & Rachford, H. H. 1955 *J. Soc. Indust. Appl. Math.* **3**, 28.

Plows, W. H. 1968 *Phys. Fluids*, **11**, 1593.

Randall, J. D. & Leibovich, S. 1973 *J. Fluid Mech.* **58**, 495.

Roache, P. J. 1972 *Computational Fluid Dynamics*. Albuquerque, N.M.: Hermosa Publishers.

Sarpkaya, T. 1971*a* *J. Fluid Mech.* **45**, 545.

Sarpkaya, T. 1971*b* *A.I.A.A. J.* **9**, 1792.

Sarpkaya, T. 1974 *A.I.A.A. J.* **12**, 602.

Squire, H. B. 1960 *Imperial College, Department of Aeronautics, Rep.* no. 102.

Torrance, K. E. 1968 *J. Res. N.B.S.* B **72**, 281.

Torrance, K. E. & Kopecky, R. M. 1971 *N.A.S.A. CR*-1867.

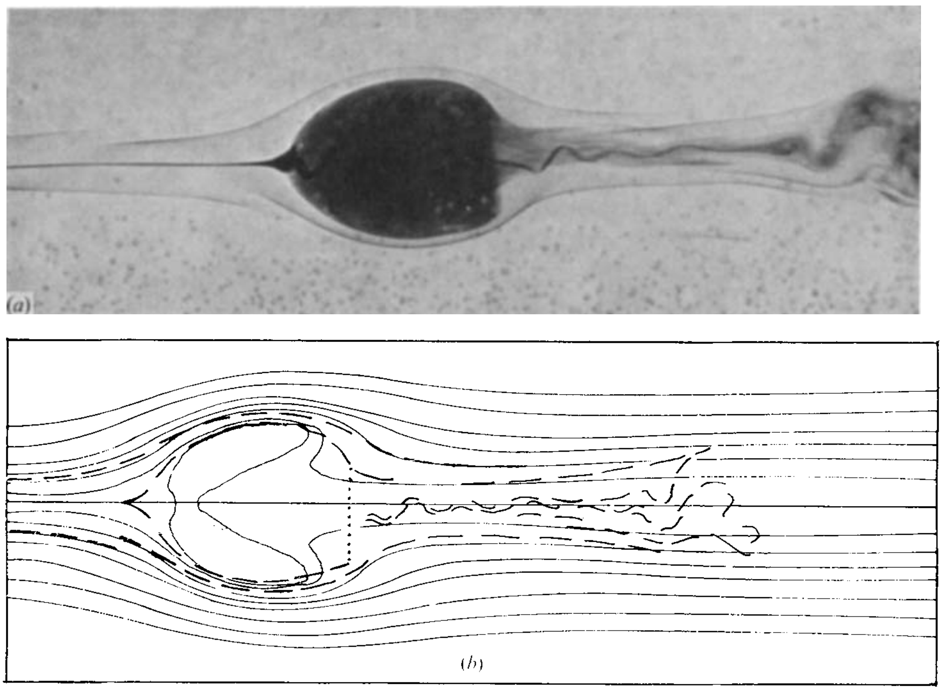

FIGURE 2. (*a*) Axisymmetric bubble followed by spiral breakdown (from Sarpkaya 1971*a*). (*b*) Comparison of stream function contours, traced from (*a*), with those calculated for $Re = 200, \alpha = 1, V = 1{\cdot}095$. The latter are uniformly scaled, for best geometric agreement. Location of spiral breakdown roughly coincides with calculated secondary stream surface divergence.